Probing the influence of incomplete fusion in the ^{6}Li $+ ^{89}$Y reaction up to 7.2 MeV/nucleon energy

Rinku Prajapat ● and Moumita Maiti ●*

Department of Physics, Indian Institute of Technology Roorkee, Roorkee-247667, Uttarakhand, India

The nuclear reaction study with weakly bound heavy nuclei is an enduring open question due to the scarcity of experimental data. In view of this, an experiment has been performed to study the fusion dynamics of weakly bound ^{6}Li projectile in ^{6}Li $+ ^{89}$Y reaction at energies slightly above the Coulomb barrier. The off-beam γ-spectroscopic technique has been used to measure the cross sections of populated residues in ^{6}Li $+ ^{89}$Y reaction, and the data are analyzed using equilibrium and pre-equilibrium models in the framework of the EMPIRE3.2.2 code. It has been found that complete fusion (CF) and incomplete fusion (ICF) of ^{6}Li play a substantial role in producing the residues. Subsequently, the ICF cross section, which is a model-dependent quantity, has been extracted. The strength of incomplete fusion has been deduced and compared with the existing data from ^{7}Li $+ ^{89}$Y reaction. The ICF strength is found to be higher for ^{6}Li $+ ^{89}$Y as compared with the ^{7}Li $+ ^{89}$Y system, which possibly indicates the role of the projectile's structure on the ICF occurrence probability. The occurrence of ICF below a critical angular momentum is also anticipated for both ^{6}Li and ^{7}Li interaction with ^{89}Y.

I. INTRODUCTION

A collision between two heavy nuclei may lead to the major nuclear reaction processes in a semiclassical picture, like compound nucleus (CN) or fusion and direct reactions, depending upon the impact parameter and interaction time. Among others, the breakup effect of the weakly bound projectile in heavy-ion fusion reactions has gained attention, both in theory and experiment, particularly due to the weak binding of stable projectiles, ^{6}Li ($\alpha + d$, $S_\alpha = 1.474$ MeV), ^{7}Li ($\alpha + t$, $S_\alpha = 2.468$ MeV), and ^{9}Be ($\alpha + \alpha + n$, $S_n = 1.665$ MeV), in the past few years [1–19]. Therefore, various processes may occur in the reaction dynamics of weakly bound nuclei, such as complete-incomplete fusion (CF-ICF), elastic-nonelastic breakup, and breakup followed by transfer mechanism. It is experimentally challenging to disentangle ICF and transfer triggered processes because the final fusion products from both the mechanisms are the same, especially in inclusive measurements.

The binary breakup of ^{6}Li can occur through the following processes [7,11,12,15,17]: (i) direct breakup from nonresonant states in continuum, (ii) instant excitation of ^{6}Li and break up into its constituent fragments α and d, termed *prompt breakup*, or excitation of ^{6}Li into relatively long-lived resonance states (1^+, 2^+, 3^+, etc.) followed by dissociation into $\alpha + d$, defined as *delayed breakup*, (iii) break up into $\alpha + p$ (^{5}Li), $\alpha + n$ (^{5}He), and $\alpha + \alpha$ (^{8}Be) triggered by n, p stripping from ^{6}Li, and d pickup by ^{6}Li, respectively. Since half-lives ($T_{1/2}$) of 1^+ and 2^+ resonance states of ^{6}Li is $\approx 1.56 \times 10^{-22}$ s and $\approx 3.8 \times 10^{-22}$ s, which are lesser than the typical collision time (10^{-21} s), it can dissociate before reaching the target (prompt breakup) and may affect the fusion, while $T_{1/2}$ of 3^+ resonance state is $\approx 2.74 \times 10^{-20}$, which is one order of magnitude longer than the collision time, hence it may break up when the collision is over and would not influence the fusion cross section. Thus, 3^+ state would contribute to CF but not to ICF. Resonance couplings play a crucial role in total fusion compared with the nonresonant couplings [15]. However, Santra *et al.* [7] suggested that delayed breakup from the resonant state (3^+, 2.186 MeV) of ^{6}Li predominates over the direct prompt breakup. They also observed that transfer followed by breakup cross section in ^{6}Li $\rightarrow ^5$Li $\rightarrow \alpha + p$ channel was comparable to the resonant breakup from 3^+ state.

In general, complete fusion cross sections of weakly bound nuclei show a significant suppression at energies above the Coulomb barrier compared with the one-dimensional barrier penetration model (1D-BPM) or coupled-channels calculations [3,5,6,9]. The breakup couplings in the continuum produce a repulsive polarization potential that enhances the fusion barrier height and suppresses the CF cross section at above-barrier energies [1]. However, total fusion cross section (TF = CF + ICF) is not influenced by the breakup process [6]. A couple of studies have been carried out by different groups in this direction, such as Kumawat *et al.* [5], who observed $\approx 34 \pm 8 \%$ suppression in CF at above-barrier energies in the ^{6}Li $+ ^{90}$Zr system, while it was reported $\approx 25\%$ for the ^{6}Li $+ ^{96}$Zr system by Hu *et al.* [3]. Later, Hu *et al.* [4] measured the cross section for one-neutron stripping from ^{6}Li to ^{96}Zr target and found that the magnitude of the transfer cross section is the same as the CF cross section at barrier energies, and extrapolation of their data confirm the predominance of transfer channel over CF at subbarrier energies. In this series,

---

*Corresponding author: moumita.maiti@ph.iitr.ac.in

TABLE I. Nuclear spectroscopic data [31] of the populated residues in ^{6}Li + ^{89}Y reaction.

Residue	J^π	$T_{1/2}$	Decay mode (%)	E_γ (keV)	I_γ (%)
^{93m}Mo	$21/2^+$	6.85 h	IT[a] (99.88)	263.05	57.4
			ϵ[b] $+ \beta^+$ (0.12)	684.69	99.9
				1477.14	99.1
^{91}Mo	$9/2^+$	15.49 min	$\epsilon + \beta^+$ (100)	1581.5	0.226
				1637.3	0.329
^{90}Mo	0^+	5.56 h	$\epsilon + \beta^+$ (100)	257.34	78.0
^{92m}Nb	2^+	10.15 d	$\epsilon + \beta^+$ (100)	934.44	99.15
^{90}Nb	8^+	14.6 h	$\epsilon + \beta^+$ (100)	132.716	4.13
				141.178	66.8
				1129.224	92.7
				2318.959	82.0
^{89m}Zr	$1/2^-$	4.161 min	IT (93.77), $\epsilon + \beta^+$ (6.23)	587.8	89.62
^{89}Zr	$9/2^+$	78.41 h	$\epsilon + \beta^+$ (100)	909.15	99.04
^{88}Zr	0^+	83.4 d	$\epsilon + \beta^+$ (100)	392.87	97.29
^{90m}Y	7^+	3.19 h	IT (100), β^- (1.8×10^{-3})	202.53	97.3
				479.51	90.74
^{87m}Y	$9/2^+$	13.37 h	IT (98.43), $\epsilon + \beta^+$ (1.57)	380.79	78.05
^{87m}Sr	$1/2^-$	2.815 h	IT (99.7), $\epsilon + \beta^+$ (0.3)	388.531	82.19

[a]Isomeric transition.
[b]Electron capture.

Zhang *et al.* [10] also estimated one-neutron stripping cross sections in the ^{89}Y(^{6}Li, ^{5}Li) ^{90}Y* reaction at $E_{lab} = 22$ and 34 MeV. Hence, it is necessary to measure the fusion cross section in the ^{6}Li + ^{89}Y reaction to disentangle the fusion and transfer processes near barrier energies.

According to the Wilczynski's Sum-Rule model [20,21], ICF usually occurs when the driving input angular momentum ℓ is greater than the critical angular momentum ℓ_{crit}. However, in a recent review [2] on ICF reactions that use cluster structured weakly and strongly bound nuclei, it has been pointed out that a substantial amount of ICF occurred below ℓ_{crit}, which contradicts Wilczynski's Sum-Rule model. In addition,

FIG. 1. A typical γ-ray spectrum of the 42.7 MeV ^{6}Li irradiated ^{89}Y collected 23 min after the EOB. The energy of the γ-ray peaks is in keV.

it is also inferred that there is a limited understanding of ICF on different entrance channel parameters, like projectile energy, structures of the colliding nuclei, projectile-target mass asymmetry μ, α-separation energy (or α-Q value), and the Z_pZ_t factor. For example, Gomes *et al.* [22] revealed that the probability of ICF (P_{ICF}) decreases with decreasing target charge (Z_t) for ^{9}Be-induced reactions, which is contradictory to the study carried out by Jha *et al.* [23]. Similarly, no systematics of the target deformation parameter β on ICF has been found in the case of strongly bound nuclei induced reactions [24]. However, they have observed a clear α-Q-value dependence on ICF in ^{12,13}C-induced reactions. Our research group also made a systematic study of CF-ICF mechanisms in weakly bound ^{7}Li-induced reactions in medium to large mass targets [8,9,13,14,16] and manifested that ICF fraction strongly depends on projectile energy. Apart from CN and direct reaction mechanisms, pre-equilibrium (PEQ) emission of light particles and clusters also play an important role in heavy-ion reaction dynamics at the energy around 10 MeV/nucleon [25–29].

After a comprehensive literature review, it has become apparent that the dependence of CF and ICF processes on various entrance-channel parameters is ambiguous, especially for weakly bound projectile-induced reactions, which need to be explored. With this aim, we have made a detailed study of the CF-ICF processes in the ^{6}Li + ^{89}Y reaction within the range 3.8–7.2 MeV/nucleon. This study includes the dependence of ICF fraction on α-separation energy (S_α) of the projectiles (^{6,7}Li) in ^{89}Y, a medium-mass target. Furthermore, the role of angular momentum has been discussed to shed light on the CF and ICF processes.

The article's organization includes experimental details of the work in Sec. II and a description of model calculations in Sec. III. Section IV discusses the analysis of measured data, and finally, Sec. V concludes the report.
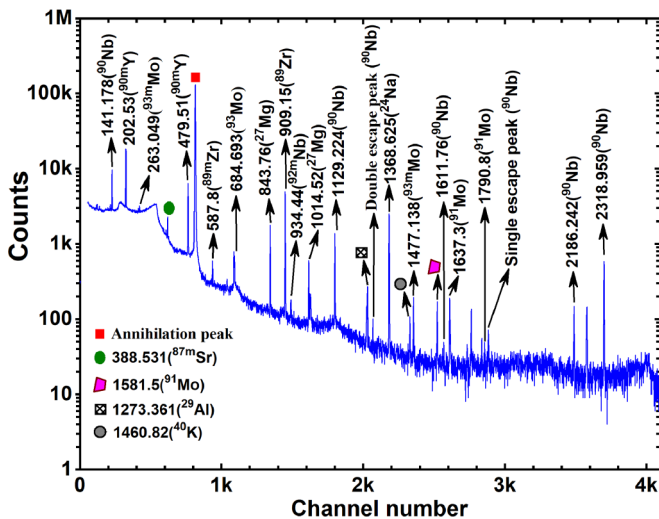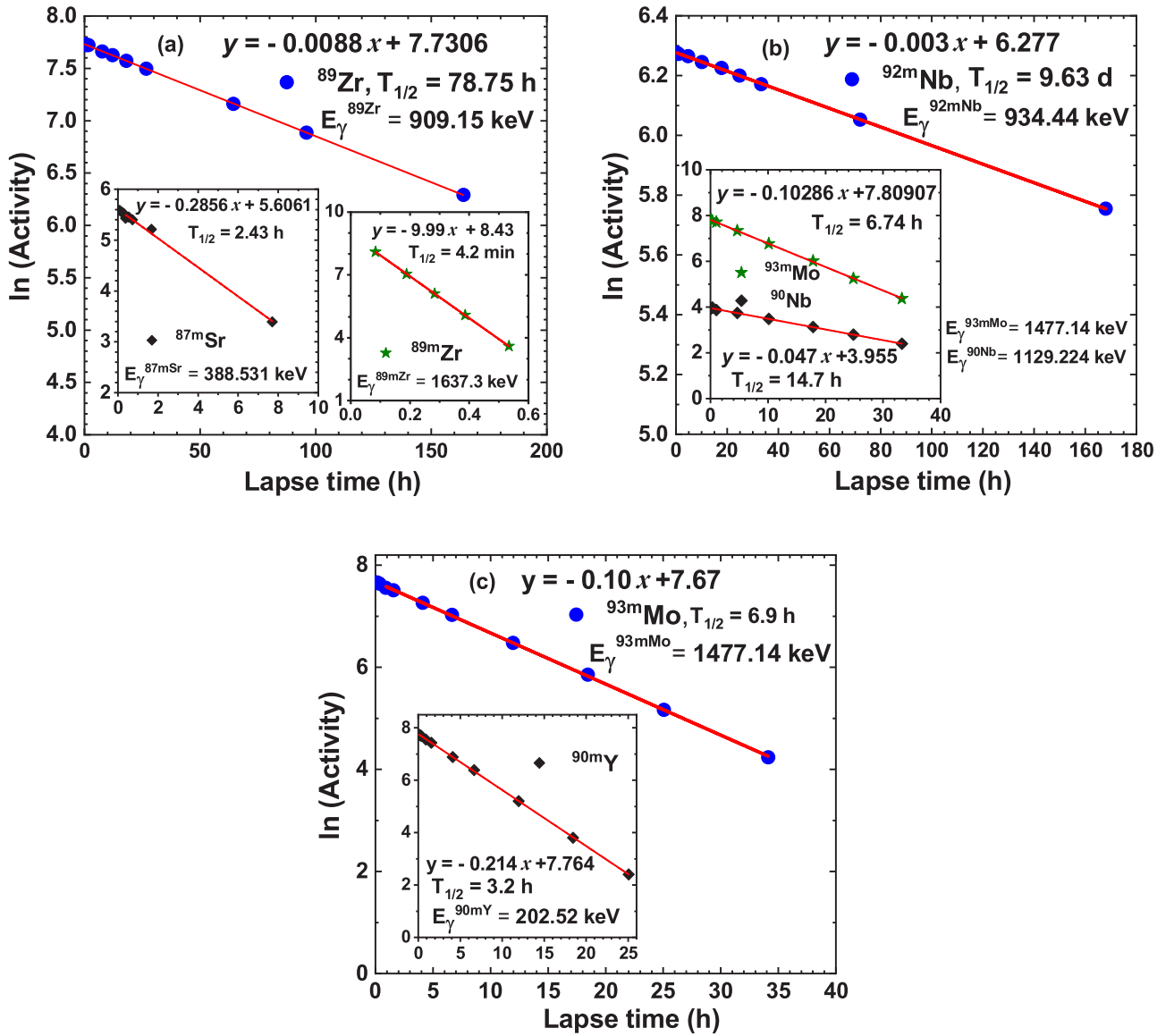
FIG. 2. Experimentally observed decay profile of (a) ^{89m,89}Zr, and ^{87m}Sr at $E_{lab} = 42.7$, (b) ^{93m}Mo, ^{92m}Nb, and ^{90}Nb at $E_{lab} = 33.5$ MeV, and (c) ^{93m}Mo and ^{90m}Y at $E_{lab} = 23.8$ MeV, populated in the ^{6}Li + ^{89}Y reaction.

II. EXPERIMENTAL DETAILS

The measurement was performed at the 14UD BARC-TIFR Pelletron facility, Mumbai, India. For the ^{6}Li + ^{89}Y fusion measurement, self-supporting pure (99.99%) natural ^{89}Y and ^{27}Al thin foils of thickness between 2.0–3.0 and 1.5–4.0 mg/cm^2, respectively, were prepared by the proper rolling method at the Pelletron target laboratory, Mumbai. In all irradiations, three Y-foils, each backed by an Al catcher foil, were assembled in a stack. The Al-catcher foils were used to stop the recoiling residues in the forward beam direction and for the incident-beam energy degradation so that suitable energy separation between the two successive target foils could be accomplished. The ^{6}Li^{3+} beam, having an energy between 23 and 43 MeV (E_{lab}), which is slightly

above the Coulomb barrier, was shot on each stack of targets. The recorded average beam flux of ^{6}Li^{3+} was $\approx 12 \times 10^{10}$ particles/s during the experiment. The beam current was maintained almost constant, and the average charge of ≈ 282 μC was collected for each irradiation setting. The total charge was measured by an electron-suppressed Faraday cup, which was installed behind the target-catcher assembly. A schematic diagram of the stack-foil arrangement can be found elsewhere in the literature [8]. The energy degradation at each foil of a stack was achieved using the Monte Carlo-simulation-based SRIM (stopping and range of ions in matter) code [30]. The energy associated with each irradiated foil is the average of the incident and outgoing energy.

After the end of bombardment (EOB), off-beam γ counting of the trapped residues, populated in the ^{6}Li + ^{89}Y
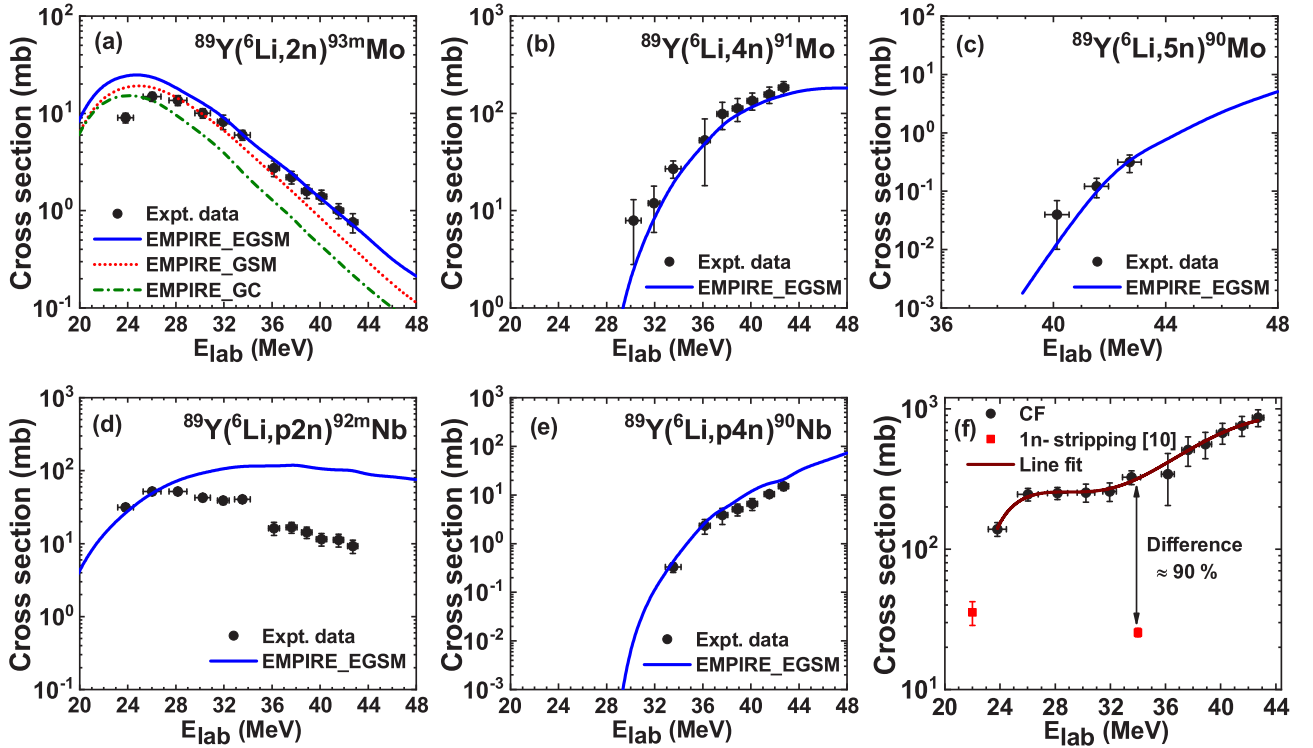
FIG. 3. Comparison between the measured excitation function of (a) ^{93m}Mo, (b) ^{91}Mo, (c) ^{90}Mo, (d) ^{92m}Nb, and (e) ^{90}Nb, and theoretical predictions from EMPIRE3.2.2, and (f) estimated CF cross section and $1n$-stripping cross section [10] for ^{6}Li $+ \, ^{89}$Y reaction at above-barrier energies. The line fit through the data is to guide the eye in panel (f).

reaction, in the target-catcher foils was done periodically by using a large-volume HPGe detector coupled with a PC-based multichannel analyzer and GENIE-2K software over a sufficiently long time to follow the decay of the residues. The detector was precalibrated by using the conventional sources ^{137}Cs (30.08 yr), ^{152}Eu (13.517 yr), and ^{60}Co (5.27 yr) of known activity. The detector's energy resolution was 2.0 keV at 1332 keV γ ray of ^{60}Co. Populated residues in each target foil (^{89}Y) were identified following their γ rays and decay-profile characteristics. The spectroscopic properties of the residues are tabulated in Table I. The unique characteristic γ rays have been used to measure the residual cross sections at each energy E using the activation relation [8,9].

The associated uncertainty in the cross-section measurement might be due to the following factors: (i) geometry-dependent efficiency of the detector, (ii) nonuniformity of target thickness, (iii) propagated error in the incident-beam flux due to fluctuation in beam current, and (iv) statistical error in the background-subtracted peak area count. The detailed quantitative error analysis due to all these factors can be found in our earlier work [8]. However, the detector's dead time was kept $\leqslant 7\%$ by adjusting the geometry of the present measurement. The total error corresponding to each cross section has been estimated by considering all these factors, and the measured data are reported in this article with up to 95% confidence level. The uncertainty associated with estimating the incident projectile energy at each foil includes the error in SRIM calculation and target-thickness determination.

III. MODEL CALCULATION

Herman *et al.* [32] has developed the statistical nuclear reaction model code EMPIRE3.2.2 to analyze various nuclear reaction mechanisms. It has been used in the present work to estimate residual cross sections from the ^{6}Li $+ \, ^{89}$Y reaction to interpret the measured data. EMPIRE predicts cross-sectional data of residues, isomeric state, and ground state. It considers various theoretical models to account for the major nuclear reaction processes involved in the heavy-ion interactions, such as optical models to estimate direct interactions, Hauser-Feshbach (HF) formalism with width fluctuation correction for compound nucleus (CN) reactions, and the exciton model (EM) or the hybrid Monte Carlo simulation model for pre-equilibrium emission calculations. Although EMPIRE has the quantum-mechanical PEQ models based on the multistep direct (MSD) and multistep compound (MSC) theory, they are not popularly used for heavy-ions because of inadequate understanding. The EM with mean-free path parameter PCROSS = 2.5 (optimum value) has been used to calculate PEQ emissions in the present calculation, and the HF formalism has been used to estimate the EQ cross sections of the residues with width-fluctuation correction. The level-density models have a crucial role in estimating the cross sections of residues in nuclear reactions. Hence, three phenomenological level-density models, such as the Gilbert-Cameron Model (GCM) [33], the Generalized Superfluid Model (GSM) [34], and the Enhanced Generalized Superfluid Model (EGSM) [35], have been used. The EGSM considers the more
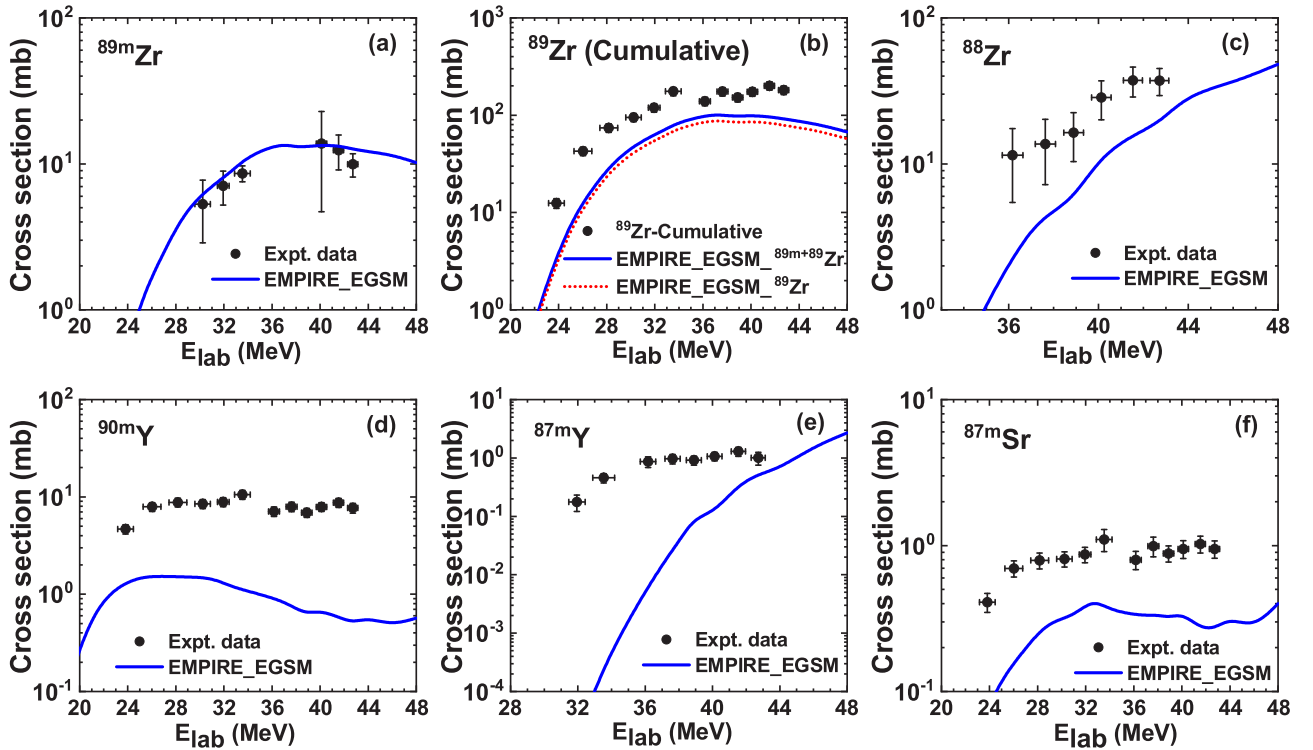
FIG. 4. Comparison between measured excitation function of (a) ^{89m}Zr, (b) ^{89}Zr (cumulative), (c) ^{88}Zr, (d) ^{90m}Y, (e) ^{87m}Y, (f) ^{87m}Sr and theoretical prediction of EMPIRE 3.2.2 with EGSM level density.

accurate treatment of angular momentum among all level-density models, which is favorable for heavy-ion-induced reactions. Some of the input parameters are selected internally from the RIPL-3 library [36], which covers nuclear masses, optical model parameters, ground-state deformations, discrete levels and decay schemes, level densities, fission barriers, and γ-ray strength functions. Some more details on EMPIRE are also available in literature [8,9,26,27].

IV. DATA ANALYSIS AND DISCUSSION

The cross sections of residues ^{93m}Mo, ^{91}Mo, ^{90}Mo, ^{92m}Nb, ^{90}Nb, ^{89m}Zr, ^{89}Zr, ^{88}Zr, ^{90m}Y, ^{87m}Y, and ^{87m}Sr, which are populated from the excited compound nuclei formed in the ^{6}Li + ^{89}Y reaction through the CF and ICF mechanism have been measured within the energy range 3.8–7.2 MeV/nucleon. A typical γ-ray spectrum of the ^{6}Li irradiated ^{89}Y target at 42.7 MeV incident energy, collected after 23 min of the EOB, has been depicted in Fig. 1, where residues are indicated corresponding to their characteristic γ peaks. The half-lives of the residues populated in each ^{89}Y foil have also been estimated from the decay data. Figures 2(a)– 2(c) represent decay profiles of some of the residues, which have lowest, moderate, and prolonged half-lives, hence estimation of half-lives at $E_{\text{lab}} = 23.8$, 33.5, and 42.7 MeV. The calculated half-lives of the residues are close to their actual half-lives [31].

The dead-time corrected and background-subtracted peak area of all the unique γ rays of each residue were analyzed to measure the activity and the residues' cross sections.

Experimentally measured cross sections, tabulated in Table II, are compared with the theory and presented in Figs. 3 and 4. The measured decay statistics with uncertainties in the area count (counts per minute) under the region of interest (peak) of each residue are also listed in Table III at E_{lab} at two extreme incident energies, 23.8 and 42.7 MeV, for easy evaluation of the reported data.

The CF and ICF cross sections and ICF fraction F_{ICF} variation against the incident energy are shown in Figs. 5(a) and 5(b). The S_{α} dependence on ICF for ^{6,7}Li + ^{89}Y systems is depicted in Fig. 6. The experimental data are shown by symbols with uncertainty, while lines represent theoretical predictions. The individual analysis of measured and theoretical excitation functions (EFs) of the residues from various reaction channels is discussed below.

A. *xn* and *pxn* channels

The measured cross sections of the ^{93m}Mo residue, which is expected to be populated by the CF mechanism ^{89}Y(^{6}Li, 2n)^{93m}Mo, has been compared with the theoretical calculations of EMPIRE (based on EQ + PEQ models) with three phenomenological level-density models EGSM, GSM, and GC, as presented in Fig. 3(a). It can be observed that predictions from EMPIRE with GSM are very close to the measured data below 31 MeV, beyond which it underestimates the data, while GC calculations underpredict the measured data throughout the energy range except at the 23.8 MeV energy. However, a reasonable agreement between EMPIRE with EGSM predictions and the measured cross section of
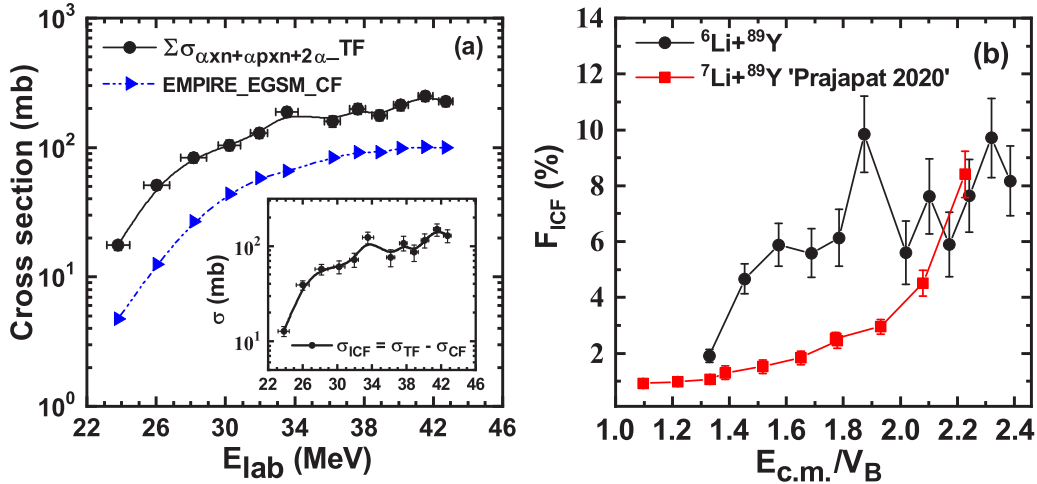
FIG. 5. (a) Variation of TF, CF, and ICF cross sections for the α-emitting channels and (b) ICF fraction (%) as a function of reduced projectile energy ($E_{c.m.}/V_B$) for ^{6}Li + ^{89}Y, and ^{7}Li + ^{89}Y; "Prajapat 2020" [8], where V_B represents the fusion barrier.

^{93m}Mo is observed over the whole energy range except below 26.0 MeV. Thus, production of the $2n$ channel residue is expected from PEQ and EQ neutrons. A similar trend of the cross-section data was reported for the $3n$ channel residues in many heavy-ion-induced reactions [25–27,29]. A critical observation suggests that EMPIRE predictions with the EGSM level density offer the best result in this case and for other xn- and pxn-channel residues. Hence, EMPIRE calculations with EGSM level density have been implemented to compare all the fellow residues.

Figures 3(b) and 3(c) show the comparison between measured cross sections of ^{91,90}Mo and theoretical predictions from EMPIRE, respectively. One can see that the measured cross section is successfully reproduced by EMPIRE with
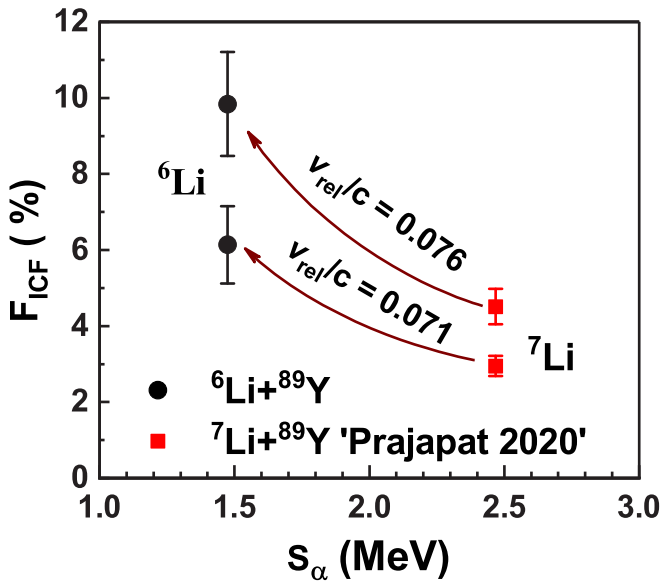

FIG. 6. Comparison of F_{ICF} (%) of ^{6}Li + ^{89}Y with the existing data of ^{7}Li + ^{89}Y reaction; "Prajapat 2020" [8], at two relative velocities, $v_{rel}/c = 0.071$ and 0.076.

EGSM, which yields production of ^{91,90}Mo via the CF mechanism. It is notable here that, due to the short half-life of ^{91}Mo and low-intensity γ rays along with low statistics of ^{91,90}Mo residues, a large uncertainty in the measured cross section is observed.

Similarly, measured EFs of ^{92m,90}Nb and those resulting from EMPIRE through the $p2n$ and $p4n$ channels are projected in Figs. 3(d) and 3(e), respectively. The measured cross sections of ^{92m}Nb are, beyond 28 MeV, significantly lower than the theoretical estimations, reproduced by the theory only at two lower-energy points. However, EF of ^{90}Nb is grossly reproduced by EMPIRE with EGSM throughout the energy range. No visible reason could be found for such low cross sections measured for ^{92m}Nb in this study. As a result, it can be concluded that the population of xn and pxn channels are through the CF mechanism, which is successfully explained by the EQ- and PEQ-model-based theory in the EMPIRE framework.

Zhang *et al.* [10] measured the one-neutron stripping cross section from ^{6}Li to ^{89}Y target using the in-beam and off-beam γ-ray spectroscopic methods at $E_{lab} = 22$ MeV and 34 MeV. To compare transfer and fusion processes at near- and above-barrier energies, the CF cross section is required for the ^{6}Li + ^{89}Y reaction. Since the present work has been carried out using off-beam γ-ray spectroscopy, some residues could not be measured due to their short half-lives or large stability. Thus, missing CF cross section has been estimated from EMPIRE (EGSM). The ratio $R = \sum_x \sigma_{xn+pxn}^{EMPIRE} / \sigma_{fus}^{EMPIRE}$, was calculated and the total CF was estimated as $\sigma_{CF} = \sum_x \sigma_{xn+pxn}^{expt}/R$, where $x = 2$, 4, and 5 for xn channels, $x = 2$ and 4 for pxn channels. The estimated total CF cross sections in the present study, which also includes CF contribution in the α-emitting channels, and $1n$-stripping cross sections from Ref. [10] are shown in Fig. 3(f). One can notice that the relative difference between the cross sectional data is ≈90% at $E_{lab} \approx 34$ MeV, a similar relative difference in CF and $1n$-stripping cross section was observed in ^{6}Li + ^{96}Zr reaction [4] at above-barrier energies. Although we have not measured CF

TABLE II. Cross sections of residues populated in the ^{6}Li + ^{89}Y reaction at various incident energies.

Series						Cross section (mb)					
Energy (MeV)	^{93m}Mo	^{91}Mo	^{90}Mo	^{92m}Nb	^{90}Nb	^{89m}Zr	^{89}Zr$_{cum}$	^{88}Zr	^{90m}Y	^{87m}Y	^{87m}Sr
23.8 ± 0.7	9.0 ± 1.0			31.4 ± 3.6			12.5 ± 1.4		4.7 ± 0.5		0.41 ± 0.06
26.0 ± 0.7	14.9 ± 1.6			52.0 ± 5.6			42.7 ± 4.4		7.9 ± 0.8		0.70 ± 0.09
28.2 ± 0.7	13.6 ± 1.6			51.8 ± 5.6			74.1 ± 7.3		8.8 ± 0.9		0.79 ± 0.10
30.2 ± 0.6	10.0 ± 1.1	7.9 ± 5.1		42.5 ± 4.8			95.0 ± 9.4		8.5 ± 0.9		0.81 ± 0.10
31.9 ± 0.5	8.2 ± 1.4	11.9 ± 6.0		38.8 ± 4.6		5.3 ± 2.4	119.4 ± 11.8		8.9 ± 0.9	0.18 ± 0.06	0.87 ± 0.11
33.5 ± 0.6	6.0 ± 0.7	27.0 ± 5.4		40.5 ± 4.5	0.33 ± 0.07	7.1 ± 1.9	175.6 ± 17.0		10.6 ± 1.1	0.46 ± 0.08	1.10 ± 0.19
36.2 ± 0.5	2.7 ± 0.5	53.0 ± 34.9		16.3 ± 3.3	2.35 ± 0.8	8.6 ± 1.1	139.1 ± 14.1	11.5 ± 6.0	7.1 ± 0.8	0.87 ± 0.18	0.80 ± 0.12
37.6 ± 0.4	2.2 ± 0.3	98.9 ± 30.8		16.7 ± 2.8	3.9 ± 1.4		175.4 ± 17.7	13.7 ± 6.5	7.9 ± 0.9	0.97 ± 0.18	0.99 ± 0.15
38.9 ± 0.4	1.59 ± 0.25	112.2 ± 29.8		14.3 ± 2.5	5.1 ± 1.4		151.9 ± 15.5	16.4 ± 6.0	6.9 ± 0.7	0.92 ± 0.16	0.88 ± 0.11
40.1 ± 0.4	1.40 ± 0.23	134.8 ± 26.9	0.040 ± 0.03	11.5 ± 2.2	6.6 ± 1.8	13.8 ± 9.1	173.9 ± 17.4	28.5 ± 8.5	7.9 ± 0.8	1.07 ± 0.18	0.95 ± 0.13
41.5 ± 0.4	1.0 ± 0.18	156.3 ± 30.0	0.12 ± 0.045	11.2 ± 2.3	10.4 ± 1.5	12.4 ± 3.3	200.9 ± 20.0	37.4 ± 8.7	8.7 ± 0.9	1.29 ± 0.23	1.02 ± 0.14
42.7 ± 0.4	0.76 ± 0.17	183.8 ± 28.0	0.31 ± 0.105	9.3 ± 1.9	15.1 ± 2.7	9.9 ± 1.8	180.7 ± 18.1	37.2 ± 7.9	7.7 ± 0.9	1.01 ± 0.25	0.95 ± 0.13

at $E_{lab} = 22$ MeV, yet if one extrapolates the measured data, then possibly the magnitude of both the cross sections would be comparable. It indicates that transfer and CF are equivalent at near-barrier energies and that transfer is a dominant process at subbarrier energies over CF [4].

B. α-emitting channels

The measured EFs of individual residues ^{89m}Zr, ^{89}Zr$_{cumulative}$, ^{88}Zr, ^{90m,87m}Y, and ^{87m}Sr, which were predominantly expected to get populated via α-emitting channels from the CN formed after the complete fusion of ^{6}Li in ^{89}Y, are shown in Figs. 4(a)–4(f) and compared with the theoretical estimations of EMPIRE with EGSM. EMPIRE calculations have been performed with the same set of input parameters, which are used to reproduce the EFs of xn and pxn channel residues and, in turn, confirmed their production via the CF mechanism. However, it can be observed from Fig. 4 that measured EFs of ^{89,88}Zr, ^{90m,87m}Y, and ^{87m}Sr show a significant enhancement as compared with EMPIRE whereas measured cross sections of ^{89m}Zr are grossly reproduced by model predictions. It is worthwhile to mention that ^{89}Zr could be populated through two reaction paths: (i) direct channel, ^{89}Y(^{6}Li, $\alpha 2n$)^{89}Zr, and (ii) indirectly through the decay of its short-lived metastable state, ^{89m}Zr, ^{89}Y(^{6}Li, $\alpha 2n$)^{89m}Zr → ^{89}Zr through IT (93.77%). The measured ^{89}Zr cross sections are thus cumulative. Hence, measured ^{89}Zr cross sections have been compared with the sum of ^{89}Zr and ^{89m}Zr cross sections obtained from EMPIRE, presented in Fig. 4(b). Although the difference between theory and experiment has been reduced a little, measured cross sections are still larger than those expected from the model. Since EMPIRE does not consider the contribution from ICF of a projectile, the observed enhancement in measured cross sections of α-emitting channels may be attributed to the ICF or transfer processes. Therefore, it is worth mentioning that the residues expected from the α-emitting channels may emerge from both CF and ICF mechanisms.

Let us look into the details of CF and ICF channels. Due to its low breakup threshold and cluster structure, the ^{6}Li projectile may break up into fragments in the nuclear field of target nuclei. This breakup process can be direct ($\alpha + d$) or sequential. The sequential breakup of ^{6}Li occurs either from an excited inelastic resonance state or a few nucleon transfers with the target nuclei before their dissociation into fragments. Hence large production cross sections of ^{89,88}Zr, ^{90m,87m}Y, and ^{87m}Sr could be due to the interplay of CF and ICF processes as described below.

CF: The complete fusion of ^{6}Li in ^{89}Y gives rise to the production of ^{95}Mo* CN in the excited state, which may eventually deexcite through the emission of light particles (e.g., p, n, α) and produce residual nuclei (Table IV).

ICF: ^{6}Li likely breaks up into constituent fragments ($\alpha + d$) in the nuclear force field of ^{89}Y. If one of the fragments fuses with the target nucleus, it populates a reduced CN, and the remaining one flies away in the forward direction as a spectator. The ICF and transfer followed by breakup-fusion mechanisms could be responsible for the large cross section of ^{89,88}Zr, ^{90m,87m}Y, and ^{87m}Sr in the ^{6}Li + ^{89}Y reaction. A

TABLE III. Measured counting statistics of residues populated in ^{6}Li + ^{89}Y reaction at E_{lab} = 23.8 and 42.7 MeV. The energy of γ rays (E_γ), shown below the radionuclides, is in keV.

Series Lapse time (h)	^{93m}Mo (1477.14)	^{91}Mo (1637.3)	^{90}Mo (257.34)	^{92m}Nb (934.44)	^{90}Nb (1129.224)	^{89m}Zr (587.8)	^{89}Zr$_{cum}$ (909.15)	^{88}Zr (392.87)	^{90m}Y (202.53)	^{87m}Y (380.79)	^{87m}Sr (388.531)
						E_{lab} = 23.8 ± 0.7					
0.1	4003 ± 28			779 ± 12			964 ± 14		18830 ± 61		872 ± 13
0.2	3962 ± 28			779 ± 12			963 ± 14		18421 ± 61		854 ± 13
0.3	3908 ± 28			779 ± 12			962 ± 14		17882 ± 60		829 ± 13
0.9	3610 ± 27			777 ± 12			886 ± 13		15481 ± 56		748 ± 12
1.6	3425 ± 26			776 ± 12			873 ± 13		13734 ± 52		632 ± 11
4.1	2682 ± 23			770 ± 12			931 ± 14		7999 ± 40		377 ± 9
6.6	2124 ± 21			765 ± 12			903 ± 13		4841 ± 31		221 ± 7
12.0	1221 ± 16			753 ± 12			871 ± 13		1490 ± 17		72 ± 4
18.4	658 ± 11			740 ± 12			837 ± 13		367 ± 9		
25.1	329 ± 8			726 ± 12			779 ± 12		91 ± 4		
34.1	130 ± 5			707 ± 12			716 ± 12				
70.8				637 ± 11			528 ± 10				
170.1				480 ± 10			227 ± 7				
						E_{lab} = 42.7 ± 0.4					
0.1	242 ± 7	506 ± 10	263 ± 7	392 ± 9	1733 ± 19	6730 ± 37	6139 ± 35	97 ± 4	15934 ± 56	277 ± 7	1125 ± 15
0.2	239 ± 7	382 ± 9	260 ± 7	391 ± 9	1724 ± 19	2357 ± 22	6133 ± 35	97 ± 4	15590 ± 56	276 ± 7	1092 ± 15
0.3	237 ± 7	296 ± 8	257 ± 7	390 ± 9	1717 ± 19	917 ± 14	6128 ± 35	97 ± 4	15288 ± 55	275 ± 7	1063 ± 15
0.4	231 ± 7	225 ± 7	254 ± 7	388 ± 9	1687 ± 18	328 ± 8	6048 ± 35	97 ± 4	14947 ± 55	276 ± 7	966 ± 14
0.5	231 ± 7	151 ± 5	249 ± 7	387 ± 9	1696 ± 18	75 ± 4	6115 ± 35	97 ± 4	14511 ± 54	271 ± 7	989 ± 14
0.7	227 ± 7	58 ± 3	243 ± 7	384 ± 9	1680 ± 18		6105 ± 35	97 ± 4	13948 ± 53	269 ± 7	937 ± 14
1.7	210 ± 6		216 ± 7	106 ± 5	1632 ± 18		6096 ± 35	97 ± 4	11885 ± 49	269 ± 7	776 ± 12
7.7	113 ± 5		102 ± 5	83 ± 4	1192 ± 15		5743 ± 34	97 ± 4	3134 ± 25	249 ± 7	126 ± 5
12.1	73 ± 4			269 ± 7	969 ± 14		5534 ± 33	97 ± 4	1320 ± 16	198 ± 6	
18.1				223 ± 7	723 ± 12		5248 ± 32	97 ± 4	378 ± 9	156 ± 6	
26.7				96 ± 4	476 ± 8		4905 ± 27	96 ± 4	64 ± 3	117 ± 5	
64.4				79 ± 4	76 ± 4		3476 ± 26	94 ± 4		77 ± 3	
96.0							2645 ± 23	94 ± 4			
163.9							1457 ± 17	92 ± 4			

quantitative analysis of the ICF has been discussed in the next section.

(1) The fusion of α-particle (α-ICF), a direct breakup fragment of ^{6}Li, leads to the formation of ^{93}Nb*, which may emit n and p to form ^{89,88}Zr, ^{90m,87m}Y, and ^{87m}Sr (Table IV), and d moves with the proportional velocity as a spectator. Similarly, fusion of d (d-ICF) in ^{89}Y may also result to the production of ^{89,88}Zr, ^{90m,87m}Y, and ^{87m}Sr (Table IV) via xn and pxn channels, respectively.

TABLE IV. CF and ICF reaction channels and the corresponding Q values.

CF of ^{6}Li		ICF of ^{6}Li (^{6}Li → α + d)	
Reaction	Q value (MeV)	Reaction	Q value (MeV)
^{89}Y(^{6}Li, 2n) ^{93m}Mo	−2.96	^{89}Y(α, $p3n$) ^{89}Zr	−31.91
^{89}Y(^{6}Li, 4n) ^{91}Mo	−23.70	^{89}Y(α, $p4n$) ^{88}Zr	−41.23
^{89}Y(^{6}Li, 5n) ^{90}Mo	−33.81	^{89}Y(α, $2pn$) ^{90m}Y	−21.44
^{89}Y(^{6}Li, $p2n$) ^{92m}Nb	−10.60	^{89}Y(α, $2p4n$) ^{87m}Y	−49.13
^{89}Y(^{6}Li, $p4n$) ^{90}Nb	−30.53	^{89}Y(α, αpn) ^{87m}Sr	−18.19
^{89}Y(^{6}Li, $\alpha 2n$) ^{89}Zr	−7.31	^{89}Y(d, 2n) ^{89}Zr	−5.84
^{89}Y(^{6}Li, $\alpha 3n$) ^{88}Zr	−16.63	^{89}Y(d, 3n) ^{88}Zr	−15.16
^{89}Y(^{6}Li, αp) ^{90m}Y	3.16	^{89}Y(d, p) ^{90m}Y	4.63
^{89}Y(^{6}Li, $\alpha p3n$) ^{87m}Y	−24.53	^{89}Y(d, $p3n$) ^{87m}Y	−23.06
^{89}Y(^{6}Li, 2α) ^{87m}Sr	6.41	^{89}Y(d, $2p2n$) ^{87m}Sr	−20.41

However, the production possibility of residues through $d + {}^{89}\text{Y}$ reaction is more likely, except for ${}^{87m}\text{Sr}$, due to their low reaction Q value. Likewise, d capture was found to be dominant over α capture at below and above the Coulomb barrier energies in the ${}^{6}\text{Li} + {}^{124}\text{Sn}$ reaction [18].

(2) There might be a chance of one-neutron stripping from ${}^{6}\text{Li}$ to ${}^{89}\text{Y}$ in the nuclear field, which leads to the formation of ${}^{90}\text{Y}^{*}$ (or ${}^{90m}\text{Y}^{*}$) and ${}^{5}\text{Li}$, which may dissociate into $\alpha + p$. The Q values for neutron transfer reactions, ${}^{89}\text{Y}({}^{6}\text{Li}, {}^{5}\text{Li}/(\alpha + p)){}^{90}\text{Y}$, are $+1.194$ MeV for ${}^{5}\text{Li}$ production and $+3.159$ MeV for $\alpha + p$. It signifies the probability of neutron transfer processes followed by breakup fusion. However, reaction Q values for the production of ${}^{89,88}\text{Zr}$, ${}^{90m,87m}\text{Y}$, and ${}^{87m}\text{Sr}$ through the $\alpha + {}^{89}\text{Y}$ are large. As a result, a neutron transfer contribution followed by α fusion is negligible in the ${}^{6}\text{Li} + {}^{89}\text{Y}$ reaction within the energy range studied. Zhang *et al.* [10] had measured the one-neutron stripping cross section from ${}^{6}\text{Li}$ to ${}^{89}\text{Y}$ explicitly.

(3) One-proton stripping [17] from ${}^{6}\text{Li}$ to ${}^{89}\text{Y}$ leads to the formation of ${}^{90}\text{Zr}^{*}$ and ${}^{5}\text{He}$, which possibly breaks up into $\alpha + n$. The populated ${}^{90}\text{Zr}^{*}$ will subsequently decay via particle or gamma emission and a possible reaction would be ${}^{6}\text{Li} + {}^{89}\text{Y} \rightarrow {}^{5}\text{He} + {}^{90}\text{Zr}^{*}$ ($Q = +3.765$ MeV) $\rightarrow \alpha + n + {}^{90}\text{Zr}^{*}$ ($Q = +4.655$ MeV). However, Castaneda *et al.* [19] reported that almost 50% of inclusive α can be interpreted by the production of ${}^{6}\text{Li} \rightarrow \alpha + d$ and ${}^{6}\text{Li} \rightarrow {}^{5}\text{He} \rightarrow \alpha + n$ exclusive breakup channels in the ${}^{6}\text{Li} + {}^{197}\text{Au}$ system. They assumed that $1p$ stripping followed by breakup ${}^{6}\text{Li} \rightarrow {}^{5}\text{He} \rightarrow \alpha + n$ cross sections are same as $1n$ stripping followed by breakup ${}^{6}\text{Li} \rightarrow {}^{5}\text{Li} \rightarrow \alpha + p$.

(4) There might be a probability of d pickup by ${}^{6}\text{Li}$ from the target, which will lead to ${}^{8}\text{Be}$ ($\alpha + \alpha$) and ${}^{87}\text{Sr}^{*}$. However, it has already been recognized [37] that the ground state (0^{+}) of ${}^{8}\text{Be}$ has a very long lifetime in comparison to collision time, which results in breakup (delayed breakup) far from the target nucleus and will not affect the CF suppression. Moreover, the breakup of ${}^{8}\text{Be}$ can occur from the excited resonance states, such as 2^{+}, in the vicinity of the target-like nucleus [38] and can affect the CF process. Hence, the fusion of any breakup fragment of ${}^{8}\text{Be}$ ($\alpha + \alpha$) with ${}^{89}\text{Y}$ will lead to the formation of [${}^{93}\text{Nb}^{*}$], which can follow Table IV for the production of these residues. The overall contribution from d pickup, followed by breakup fusion, will be less because it is a three-step process, but the possibility exists.

Souza *et al.* [17] measured the contribution from all singles α, d, and p production from breakup, transfer, and transfer followed by breakup processes, inclusively. Furthermore, the α-d coincidence measurements suggested that the more significant contribution is due to the direct breakup process in the ${}^{6}\text{Li} + {}^{59}\text{Co}$ system. Since we have used the off-beam γ-ray spectroscopic method, it explicitly restricts disentangling of different breakup and transfer mechanisms.

C. Analysis of incomplete fusion

Since we have deployed the γ-spectrometric technique to estimate production cross section of various populated residues in the ${}^{6}\text{Li} + {}^{89}\text{Y}$ reaction, the estimated ICF cross section is a model-dependent quantity, not purely from experiment. The enhancement in cross sections of ${}^{89,88}\text{Zr}$, ${}^{90m,87m}\text{Y}$, and ${}^{87m}\text{Sr}$ residues has been observed compared with the EMPIRE estimations, shown in Figs. 4(b)–4(f). Since EMPIRE does not consider ICF or transfer followed by ICF in its calculation kernel, the residues' population is purely from the CF mechanism in the ${}^{6}\text{Li} + {}^{89}\text{Y}$ system. Furthermore, for a better insight into ICF, the sum of experimentally measured α-emitting channels ($\sum \sigma_{\text{expt}}^{\alpha xn + \alpha pxn + 2\alpha}$) have been compared with that predicted from EMPIRE ($\sum \sigma_{\text{EMPIRE}}^{\alpha xn + \alpha pxn + 2\alpha}$), as shown in Fig. 5(a). The sum of experimental cross sections from the α channels is significantly higher than the EMPIRE predictions after deployment of the same set of input parameters used to reproduce the xn and pxn channel residues, which are mainly populated via the CF mechanism. Hence, observed enhancement in measured cross sections over EMPIRE is attributed to ICF and nucleon transfer followed by ICF mechanisms. The strength of ICF has been analyzed with the help of a data reduction method [8,9,13,14].

To deduce the extent of the ICF contribution in the ${}^{6}\text{Li} + {}^{89}\text{Y}$ reaction, the ICF cross section ($\sum \sigma_{\text{ICF}}$) has been estimated, $\sum \sigma_{\text{ICF}} = \sum \sigma_{\text{TF}}^{\alpha xn + \alpha pxn + 2\alpha} - \sum \sigma_{\text{CF}}^{\alpha xn + \alpha pxn + 2\alpha}$, where σ_{TF} (CF + ICF) and σ_{CF} are the sum of experimental and theoretical cross sections, respectively. The σ_{TF} (black line), sum of measured cross sections of ${}^{89}\text{Zr}$, ${}^{88}\text{Zr}$, ${}^{90m}\text{Y}$, ${}^{87m}\text{Y}$, and ${}^{87m}\text{Sr}$ residues, σ_{CF} (blue line), sum of theoretical cross sections of those residues obtained from EMPIRE, and ICF cross sections [black line, inset of Fig. 5(a)] (σ_{ICF}), are presented in Fig. 5(a). The estimated ICF cross section is thus a model-dependent quantity.

For a better insight into the quantification of ICF and its dependence on different entrance channel parameters, such as projectile energy and S_{α} value, ICF fraction (F_{ICF}) has been deduced. F_{ICF}, which measures the strength of ICF over CF, is defined as F_{ICF} (%) = $(\sum \sigma_{\text{ICF}}/\sigma_{\text{TF}}^{\text{theor}}) \times 100\%$, where $\sigma_{\text{TF}}^{\text{theor}}$ is the total theoretical fusion cross section (sum of all residues) predicted from EMPIRE. F_{ICF} has been plotted as a function of energy in the center-of-mass frame, $E_{\text{c.m.}}$, in Fig. 5(b). Notably, F_{ICF} is increasing with growing projectile energy.

To study the effect of entrance channel parameter (for example, projectile structure) on ICF, estimated F_{ICF} from the α-emitting channels of ${}^{7}\text{Li} + {}^{89}\text{Y}$ reaction [8] has been plotted with the ${}^{6}\text{Li} + {}^{89}\text{Y}$ system in Fig. 5(b) by scaling the energy values ($E_{\text{c.m.}}/\text{V}_{B}$), where V_{B} is the Bass barrier. One can observe that F_{ICF} is higher for ${}^{6}\text{Li}$-induced reaction as compared with ${}^{7}\text{Li}$ throughout the energy range, except at $E_{\text{c.m.}}/\text{V}_{B} = 2.23$. However, three α-channels were considered for the contribution of ICF in ${}^{7}\text{Li} + {}^{89}\text{Y}$ [8], while we could measure five α-emitting channels in the present study.

The variation in F_{ICF} for ${}^{6}\text{Li} + {}^{89}\text{Y}$ and ${}^{7}\text{Li} + {}^{89}\text{Y}$ [8] reactions indicating the effect of projectile structure as the target is the same in both cases. It is known that ${}^{6,7}\text{Li}$ both are α-cluster structured and weakly bound nuclei. However, ${}^{6}\text{Li}$

$(\alpha + d, S_\alpha = 1.474 \text{ MeV})$ has less α-separation energy (S_α) as compared with ^{7}Li ($\alpha + t$, $S_\alpha = 2.468$ MeV). Thus, ^{6}Li nuclei with less S_α pose larger breakup probability as compared with ^{7}Li. As a result, ^{6}Li + ^{89}Y system has larger F_{ICF} as compared with ^{7}Li + ^{89}Y system within the studied energy range, as seen in Fig. 5(b). A similar conclusion has been made in a recent review about the co-relation of S_α with the ICF fraction [2].

Furthermore, to make it even more clear, the F_{ICF} factor has been deduced for ^{6}Li + ^{89}Y and ^{7}Li + ^{89}Y [8] reactions at two different constant relative velocities (v_{rel}/c) = 0.071 and 0.076. The relative velocity (v_{rel}/c) has been estimated from the relation $[2(E_{c.m.} - V_B)/\mu c^2]^{1/2}$, where V_B, c, and μ are the Coulomb barrier between the interacting nuclei, speed of light, and the reduced mass of the system, respectively [39]. F_{ICF} has been plotted against S_α in Fig. 6 at a constant relative velocity. It can be seen from the figure that ICF fraction is small for high S_α value and is relatively large for low S_α, which follows the same trend as observed in Fig. 5(b). F_{ICF} is $\approx 4.5 \pm 0.5\%$ for ^{7}Li + ^{89}Y system and $\approx 9.8 \pm 1.4\%$ for ^{6}Li + ^{89}Y at a constant $v_{rel}/c = 0.076$. It indicates the role of S_α of weakly bound ^{6,7}Li nuclei to understand the breakup-fusion mechanism.

D. Role of input angular momentum

At low energies, the CF occurs due to the complete amalgamation of interacting nuclei because of the dominance of short-range attractive nuclear potential. In CF reaction, a fully equilibrated compound nucleus is formed after the equal distribution of energy and momenta among all the nucleonic degree of freedom within the input angular-momentum range $\ell < \ell_{crit}$. However, in the case of ICF reactions, only partial transfer of mass, linear and angular momenta occur and are localized in an ℓ-space with $\ell > \ell_{crit}$ as prescribed by the Sum-Rule model [20,21]. According to this model, at $\ell > \ell_{crit}$, the capture of more massive breakup fragments occurs at the beginning followed by the light fragments at higher angular momenta, and fusion of each breakup fragment with the target nucleus have their own ℓ_{crit} above which the incident fragment would be unable to fuse with the target nucleus.

For a better understanding, the critical angular momentum (ℓ_{crit}) has been simulated for the colliding system by applying equilibrium conditions between the Coulomb, nuclear, and centrifugal forces using the following simplified formula given by Wilczynski [20]:

$$\left(\ell_{crit} + \frac{1}{2}\right)^2 = \frac{\mu(C_p + C_t)^3}{\hbar^2}\left[4\pi\gamma\frac{C_p C_t}{C_p + C_t} - \frac{Z_p Z_t e^2}{(C_p + C_t)^2}\right], \quad (1)$$

where μ is the reduced mass of the interacting nuclei, γ is the surface tension coefficient, and Z_p, Z_t and C_p, C_t are the atomic numbers and half-density radii of the projectile and target nuclei, respectively. The half-density radii were estimated by using the following relation:

$$C = R\left[1 - \left(\frac{b^2}{R^2}\right) + \cdots\right]. \quad (2)$$

TABLE V. The estimated values of ℓ_{crit} and ℓ_{max} using Eqs. (4) and (3), respectively, at various incident energies for ^{6}Li + ^{89}Y and ^{7}Li + ^{89}Y [8] systems.

^{6}Li + ^{89}Y				^{7}Li + ^{89}Y			
E_{lab} (MeV)	$E_{c.m.}$ (MeV)	ℓ_{crit} ($\hbar$)	ℓ_{max} ($\hbar$)	E_{lab} (MeV)	$E_{c.m.}$ (MeV)	ℓ_{crit} ($\hbar$)	ℓ_{max} ($\hbar$)
23.8	22.3	12	11	19.4	17.9	8	6
26.0	24.4	13	13	21.5	19.9	11	10
28.2	26.4	14	15	23.5	21.8	12	12
30.2	28.3	15	16	24.5	22.7	13	13
31.9	29.9	16	17	26.8	24.8	15	15
33.5	31.4	16	18	29.1	27.0	16	17
36.2	33.9	17	19	31.3	29.0	17	18
37.6	35.3	18	20	34.1	31.6	18	20
38.9	36.4	18	21	36.7	34.0	19	22
40.1	37.6	19	21	39.4	36.5	20	23
41.5	38.9	19	22				
42.7	40.0	19	23				

Here, $b = 1$ fm and $R = 1.28A^{1/3} - 0.76 + 0.8A^{-1/3}$ fm is the equivalent sharp radius. The estimated value of ℓ_{crit} using Eq. (1) is $\approx 18\hbar$ and $\approx 21\hbar$ for the ^{6}Li + ^{89}Y and ^{7}Li + ^{89}Y [8] systems. However, if we replace the half density radii (C) by the sharp radius $R = 1.11 A^{1/3}$ fm [40], than the estimated values of ℓ_{crit} are $\approx 25\hbar$ and $\approx 28\hbar$ for the ^{6}Li + ^{89}Y and ^{7}Li + ^{89}Y systems, respectively. This suggests a range of critical angular momentum $\ell_{crit} = 18\hbar - 25\hbar$ and $21\hbar - 28\hbar$ for all the peripheral processes, such as ICF and transfer of nucleon and/or cluster in ^{6,7}Li-induced reactions in ^{89}Y, respectively, as it is known that various static and dynamical effects occur during the fusion process in the surface region of the nuclear interaction or in the tail region of the Coulomb barrier.

The maximum angular momentum ℓ_{max} can be estimated from the following relation:

$$\ell_{max} = R\sqrt{2\mu(E_{c.m.} - V_B)/\hbar^2} \quad (3)$$

where R is the maximum distance between two nuclei at which the collision leads to a reaction, and V_B is the fusion barrier at distance R. As can be observed from Eq. (1), the value of ℓ_{crit} depends on the radius parameter and independent of projectile energy. Hence, we have implemented the energy-dependent relation [41,42] for the estimation of ℓ_{crit} as given below:

$$\ell_{crit} = C_R[d_0 + d_1\sqrt{(E_{c.m.} - V_C)}]. \quad (4)$$

Here, $V_C = 1.18Z_p Z_t/(A_p^{1/3} + A_t^{1/3} + 1.6)$ MeV, $d_0 = 0.33$, and $d_1 = 0.205$ MeV^{-1}, and $C_R = \sqrt{A_p A_t/(A_p + A_t)}(A_p^{1/3} + A_t^{1/3})$. The calculated values of ℓ_{max} and ℓ_{crit} using Eqs. (3) and (4), respectively, are listed in Table V. One can notice (Table V) that, at most of the incident energies, $\ell_{crit} < \ell_{max}$ for both reactions, which indicates the occurrence of ICF at angular momentum $\ell > \ell_{crit}$ that is obvious. However, according to the Wilczynski formalism, the range of ℓ_{crit} is higher than ℓ_{max} for both the systems. It indicates that a significant portion of the ℓ window also contributes towards the ICF

mechanism at angular momentum $\ell < \ell_{\rm crit}$ as also pointed out in Ref. [24].

Furthermore, we have estimated $\ell_{\max}$ for $^6{\rm Li} + {}^{89}{\rm Y}$ and $^7{\rm Li} + {}^{89}{\rm Y}$ reactions at $E_{\rm c.m.} = 31.4$ and 31.6 MeV, respectively, using the CCFULL code [43]. The code estimates the fusion cross section and mean angular momentum for heavy-ion-induced reactions with and without coupling between the colliding partners at different $E_{\rm c.m.}$. The present calculations have been carried out without considering any couplings between the interacting nuclei using the Woods-Saxon form of nuclear potential with Akyüz-Winther (AW) parametrization such as potential depth ($V_0 = 43.3$ and 44.0 MeV), radius ($r_0 = 1.17$ and 1.17 fm), and diffuseness parameter ($a_0 = 0.61$ and 0.61 fm) for the $^6{\rm Li} + {}^{89}{\rm Y}$ and $^7{\rm Li} + {}^{89}{\rm Y}$ systems, respectively. The predicted $\ell_{\max}$ values are $\approx 17\hbar$ and $\approx 19\hbar$ for the $^6{\rm Li} + {}^{89}{\rm Y}$ and $^7{\rm Li} + {}^{89}{\rm Y}$ systems, respectively at $E_{\rm c.m.} = 31.4$ and 31.6 MeV, respectively, which are in good agreement with those calculated from Eq. (3), listed in Table V.

V. CONCLUSION

For a better understanding of CF and ICF processes involved with weakly bound projectile and ICF dependence on various entrance channel parameters, the residual cross sections in the $^6{\rm Li} + {}^{89}{\rm Y}$ reaction have been measured by using the off-beam γ-ray spectroscopic method in the 3.8–7.2 MeV/nucleon energy range. The measured cross sections of residues have been analyzed by comparing them with the theoretical model calculations based on the Hauser-Feshbach formalism for compound reactions and exciton models for PEQ emissions in the EMPIRE framework. The experimentally measured cross section of xn- and pxn-channels are successfully reproduced by EMPIRE with EGSM calculations, which ensures the production of those residues via the CF mechanism. However, a significant amount of enhancement has been observed compared with theory (CF process) in α-emitting channels, which is attributed to the ICF and/or transfer processes involved in $^6{\rm Li} + {}^{89}{\rm Y}$ reaction. ICF's strength ($F_{\rm ICF}$) has been deduced for α-emitting channels in the $^6{\rm Li} + {}^{89}{\rm Y}$ reaction, and it was found that ICF is increasing with the elevating projectile energy. It has also been observed that $F_{\rm ICF}$ is larger for the $^6{\rm Li} + {}^{89}{\rm Y}$ reaction in comparison with $^7{\rm Li} + {}^{89}{\rm Y}$ [8], which indicates the correlation of ICF with the S_α value of $^{6,7}{\rm Li}$ projectiles. Furthermore, the fusion ℓ distribution suggests an ℓ window below $\ell_{\rm crit}$ for incomplete fusion.

[1] L. F. Canto, P. R. S. Gomes, R. Donangelo, J. Lubian, and M. S. Hussein, Phys. Rep. **596**, 1 (2015).

[2] V. Jha, V. V. Parkar, and S. Kailas, Phys. Rep. **845**, 1 (2020).

[3] S. P. Hu, G. L. Zhang, J. C. Yang, H. Q. Zhang, P. R. S. Gomes, J. Lubian, X. G. Wu, J. Zhong, C. Y. He, Y. Zheng *et al.*, Phys. Rev. C **91**, 044619 (2015).

[4] S. P. Hu, G. L. Zhang, J. C. Yang, H. Q. Zhang, P. R. S. Gomes, J. Lubian, J. L. Ferreira, X. G. Wu, J. Zhong, C. Y. He *et al.*, Phys. Rev. C **93**, 014621 (2016).

[5] H. Kumawat, V. Jha, V. V. Parkar, B. J. Roy, S. K. Pandit, R. Palit, P. K. Rath, C. S. Palshetkar, S. K. Sharma, S. Thakur *et al.*, Phys. Rev. C **86**, 024607 (2012).

[6] P. R. S. Gomes, I. Padron, M. D. Rodríguez, G. V. Martí, R. M. Anjos, J. Lubian, R. Veiga, R. L. Neto, E. Crema, N. Added *et al.*, Phys. Lett. B **601**, 20 (2004).

[7] S. Santra, V. V. Parkar, K. Ramachandran, U. K. Pal, A. Shrivastava, B. J. Roy, B. K. Nayak, A. Chatterjee, R. K. Choudhury, and S. Kailas, Phys. Lett. B **677**, 139 (2009).

[8] R. Prajapat and M. Maiti, Phys. Rev. C **101**, 024608 (2020).

[9] R. Prajapat and M. Maiti, Phys. Rev. C **101**, 064620 (2020).

[10] G. L. Zhang, G. X. Zhang, S. P. Hu, Y. J. Yao, J. B. Xiang, H. Q. Zhang, J. Lubian, J. L. Ferreira, B. Paes, E. N. Cardozo *et al.*, Phys. Rev. C **97**, 014611 (2018).

[11] D. H. Luong, M. Dasgupta, D. J. Hinde, R. du Rietz, R. Rafiei, C. J. Lin, M. Evers, and A. Diaz-Torres, Phys. Lett. B **695**, 105 (2011).

[12] F. A. Souza, N. Carlin, C. Beck, N. Keeley, A. Diaz-Torres, R. L. Neto, C. Siqueira-Mello, M. M. de Moura, M. G. Munhoz, R. A. N. Oliveira *et al.*, Eur. Phys. J. A **44**, 181 (2010).

[13] D. Kumar, M. Maiti, and S. Lahiri, Phys. Rev. C **94**, 044603 (2016).

[14] D. Kumar, M. Maiti, and S. Lahiri, Phys. Rev. C **96**, 014617 (2017).

[15] A. G. Camacho, A. Diaz-Torres, and H. Q. Zhang, Phys. Rev. C **99**, 054615 (2019).

[16] A. Chauhan and M. Maiti, Phys. Rev. C **99**, 034608 (2019).

[17] F. A. Souza, C. Beck, N. Carlin, N. Keeley, R. L. Neto, M. M. de Moura, M. G. Munhoz, M. G. Del Santo, A. A. P. Suaide, E. M. Szanto *et al.*, Nucl. Phys. A **821**, 36 (2009).

[18] V. V. Parkar, S. K. Pandit, A. Shrivastava, R. Palit, K. Mahata, V. Jha, K. Ramachandran, S. Gupta, S. Santra, S. K. Sharma *et al.*, Phys. Rev. C **98**, 014601 (2018).

[19] C. M. Castaneda, H. A. Smith, Jr., P. P. Singh, and H. Karwowski, Phys. Rev. C **21**, 179 (1980).

[20] J. Wilczyński, K. Siwek-Wilczyńska, J. Van-Driel, S. Gonggrijp, D. C. J. M. Hageman, R. V. F. Janssens, J. Lukasiak, R. H. Siemssen, and S. Y. Van Der Werf, Nucl. Phys. A **373**, 109 (1982).

[21] J. Wilczyński, K. Siwek-Wilczyńska, J. van Driel, S. Gonggrijp, D. C. J. M. Hageman, R. V. F. Janssens, J. Łukasiak, and R. H. Siemssen, Phys. Rev. Lett. **45**, 606 (1980).

[22] P. R. S. Gomes, R. Linares, J. Lubian, C. C. Lopes, E. N. Cardozo, B. H. F. Pereira, and I. Padron, Phys. Rev. C **84**, 014615 (2011).

[23] V. Jha, V. V. Parkar, and S. Kailas, Phys. Rev. C **89**, 034605 (2014).

[24] H. Kumar, S. A. Tali, M. A. Ansari, D. Singh, R. Ali, A. Ali, S. Parashari, P. K. Giri, S. B. Linda, R. Kumar *et al.*, Phys. Rev. C **99**, 034610 (2019).

[25] R. Prajapat, M. Maiti, D. Kumar, and A. Chauhan, Phys. Scr. **95**, 055306 (2020).

[26] D. Kumar and M. Maiti, Phys. Rev. C **95**, 064602 (2017).

[27] A. Chauhan, M. Maiti, and S. Lahiri, Phys. Rev. C **99**, 064609 (2019).

[28] M. Maiti and S. Lahiri, Phys. Rev. C **84**, 067601 (2011).

[29] R. Prajapat, M. Maiti, and D. Kumar, Phys. Rev. C **103**, 014608 (2021).

[30] J. F. Ziegler, M. D. Ziegler, and J. P. Biersack, Nucl. Instrum. Methods Phys. Res., Sect. B **268**, 1818 (2010).

[31] National Nuclear Data Center, Brookhaven National Laboratory, http://www.nndc.bnl.gov/nudat2.

[32] M. Herman, R. Capote, B. V. Carlson, P. Oblozinsky, M. Sin, A. Trkov, H. Wienke, and V. Zerkin, Nucl. Data Sheets **108**, 2655 (2007).

[33] A. Gilbert and A. G. W. Cameron, Can. J. Phys. **43**, 1446 (1965).

[34] A. V. Ignatyuk, J. L. Weil, S. Raman, and S. Kahane, Phys. Rev. C **47**, 1504 (1993).

[35] A. D'Arrigo, G. Giardina, M. Herman, A. V. Ignatyuk, and A. Taccone, J. Phys. G: Nucl. Part. Phys. **20**, 365 (1994).

[36] R. Capote, M. Herman, P. Obložinský, P. G. Young, S. Goriely, T. Belgya, A. V. Ignatyuk, A. J. Koning, S. Hilaire, V. A. Plujko *et al.*, Nucl. Data Sheets **110**, 3107 (2009).

[37] D. J. Hinde, M. Dasgupta, B. R. Fulton, C. R. Morton, R. J. Wooliscroft, A. C. Berriman, and K. Hagino, Phys. Rev. Lett. **89**, 272701 (2002).

[38] K. J. Cook, E. C. Simpson, D. H. Luong, S. Kalkal, M. Dasgupta, and D. J. Hinde, Phys. Rev. C **93**, 064604 (2016).

[39] H. Morgenstern, W. Bohen, W. Galster, K. Grabisch, and A. Kyanowski, Phys. Rev. Lett. **52**, 1104 (1984).

[40] J. Wilczyński, Nucl. Phys. A **216**, 386 (1973).

[41] P. Fröbrich and I. I. Gontchar, Phys. Rep. **292**, 131 (1998).

[42] M. V. Chushnyakova and I. I. Gontchar, Nucl. Phys. A **941**, 255 (2015).

[43] K. Hagino, N. Rowley, and A. T. Kruppa, Comput. Phys. Commun. **123**, 143 (1999).